Newport
Experience | Solutions

The Brands of Innovation.


光学隔振平台


老化测试系统


半导体激光器


Picomotor™促动器


旋转台


光学镜片


红外及激光器配件


光源


单色仪


光栅


激光器


系统集成解决方案

联系我们

Newport中国
电话：+86 510 8113 5000

中国区代理商：科艺仪器有限公司
电话：+86 400 886 0019

Newport 官方微信

The alignment and imaging experiment of a telescope with wavefront coding technology

Feng Yan (闫 锋)

Key Laboratory of Optical System Advanced Manufacturing Technology, Changchun Institute of Optics, Fine Mechanics and Physics, Chinese Academy of Science, Changchun 130033, China

Corresponding author: yanfeng@ciomp.ac.cn

Received September 24, 2013; accepted October 17, 2013; posted online February 26, 2014

Wavefront coding (WFC) is kind of computational imaging technique that controls misfocus and misfocus-related aberrations of optical systems by appending a specially designed phase distribution to the pupil function. This technology has been applied in many fields to increase the performance or/and reduce the cost of imaging systems. The application of WFC technology on an off-axis three-mirror anastigmatic (TMA) system has been proposed in our previous work. In this letter, we describe the alignment, the imaging experiment and image restoration of an actual TMA system with WFC technology.

OCIS codes: 220.1140, 100.3020, 110.1758.

doi: 10.3788/COL201412.S12201.

The application of wavefront coding (WFC) technology enables optical-digital imaging systems the insensitivity to misfocus-related aberrations such as astigmatism, and Petzval curvature, temperature-related and alignment-related misfocus[1–3]. Due to its particular character, it has been applied in many fields such as iris recognizing, bar-code scanning, biological microscope, thermal imaging system and so on[4–7]. In our previous researching, the WFC technology has been applied on a typical Cook's TMA system (invented by Wetherell and Womble of ITEK Corp., US Patent 4240707 in Dec. 23, 1980) to extend its depth of focus (DOF). The optical design, optimization and the image restoration have been reported[8–11]. The sketch of the system and its main parameters are shown in Fig. 1. The focal length is 2 m and the selected cut-off frequency is 57.2lp/mm for 8.75 μm × 8.75 μm charge-coupled device CCD pixel, which will be used actually. The secondary mirror is selected to be the WFC element, and its surface figure is shown in

$$z(x,y)=\frac{c(x^2+y^2)}{1+\sqrt{1-(1+k)c^2(x^2+y^2)}}+\beta(x_n{}^3+y_n{}^3), \quad (1)$$

where x, y is actual coordinate and x_n, y_n is normalized coordinate. It can be seen that a cubic term is appended to the original form so as to introduce a special cubic distribution to the pupil function. The modulation transfer function (MTF) curves of the system in the extended DOF are shown in Fig. 2, from which it can be observed that the MTF values keep nearly invariant in despite of different defocus aberration.

The self-collimated alignment is applied to assembly of the system. The wavefront of only one field of view (FOV) is measured for simplicity. The surface figure error of each mirror (only within effective aperture) is about 0.025 λ root mean square (rms) (λ@632.8nm). The alignment of wavefront-coded system is a little different from usual optical system: the aligning target of usual systems is to minimize the residual wavefront while the target of wavefront-coded system is to obtain a special cubic wavefront map as shown in Fig. 3(a). For convenience, the ideal wavefront error is made in the system error file of interferometer and can be eliminated automatically from the actual wavefront in each testing, and thus the residual wavefront error between

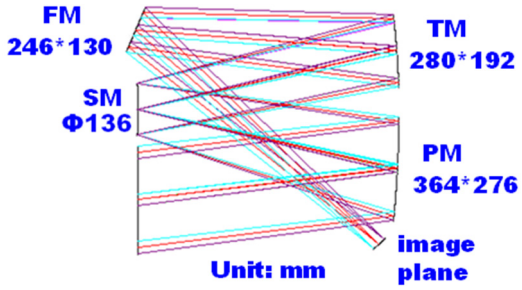

Fig. 1. The layout and main parameters of the off-axis TMA system under research, where PM is primary mirror, SM is secondary mirror, TM is tertiary mirror and FM is folded mirror.

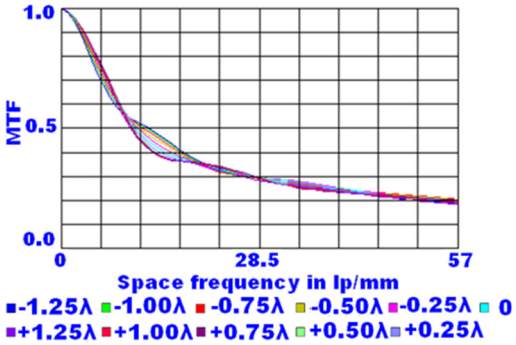

Fig. 2. The MTF curves of optimized WFC system with different defocus aberration varying from −1.25 λ to 1.25 λ with increment of 0.25 λ defocus.

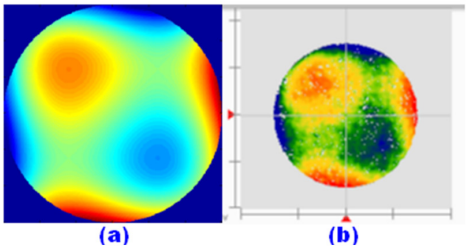

Fig. 3. (a) The ideal wavefront map of the wavefront coded system; (b) The actual wavefront map of the wavefront coded system obtained by Phasecam 5030 interferometer of 4D Corp.

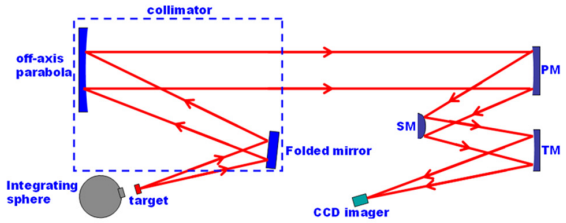

Fig. 4. Sketch of experimental setup.

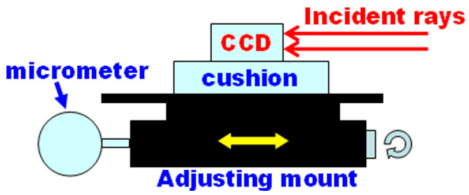

Fig. 5. Sketch of the CCD imager and its adjustment in the direction of incident chief rays.

the actual wavefront and the system error is used as the calibrating criterion. When the residual wavefront error reaches its minimum, the special cubic wavefront is obtained as shown in Fig. 3(b). It should be pointed out that in the assembly process the primary mirror is set to be the alignment benchmark and the tertiary mirror is firstly calibrated according to the primary mirror, which decreases the difficulty in assembling the secondary mirror.

Imaging experiment is carried out after alignment. The experimental setup is shown in Fig. 4. The focal length of the collimator is 4 m, and thus the magnifying ratio of the system is 2. The folded mirror of the optical system is neglected for simplification without any negative effect. The imager is FL2-20S4M-C CCD of Point Grey Corp. and the effective pixel number is 1600 × 1200 and a single pixel size is 4.4 μm × 4.4 μm. The CCD imager of relatively smaller pixel size (not 8.75 μm × 8.75 μm) is selected to catch more detail of the PSF. The CCD camera is located on a six-dimension adjusting mount. Especially, the needed defocus aberration is introduced by moving the imager along the direction of the incident chief ray forward/backward and a micrometer is used to watch the defocus amount as shown in Fig. 5. The initial position of the CCD imager is determined in aligning process, in which the actual defocus aberration W_{020} of the optical system is zero. Especially, this initial position can also be regarded as the nominal ideal image plane.

Firstly, a star point of 20 μm is imaged and totally 11-point spread function (PSF) images are caught as shown in Fig. 6(b). The size of the star point should be 8.8 μm according to the focal length of the collimator and the size of CCD pixel. But we didn't have star point of the right size at that time, so the 20-μm one is used instead. The range of defocus aberration of these

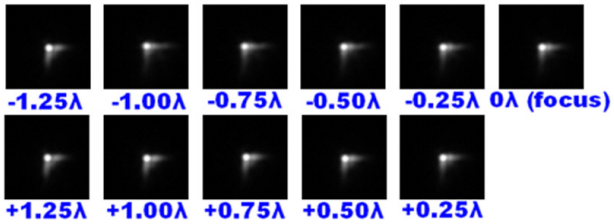

Fig. 6. The PSF image of the system with different defocus aberration from −1.25 λ to 1.25 λ.

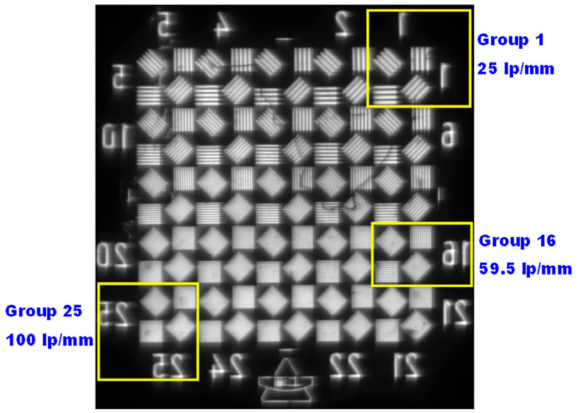

Fig. 7. The image of the third plate of WT1005-62 resolution patterns

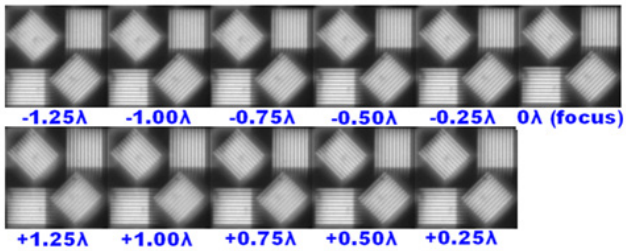

Fig. 8. Original images of the 16th group resolution pattern with different defocus aberration from −1.25 λ to 1.25 λ.

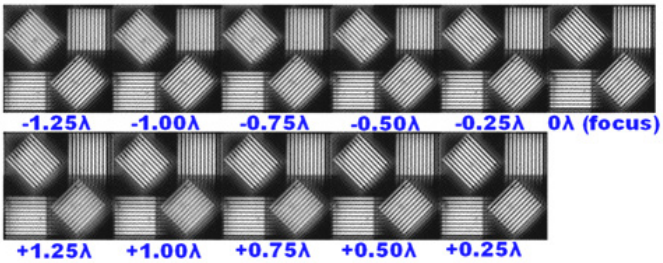

Fig. 9. Restored images of the 16th group resolution pattern with different defocus aberration from −1.25 λ to 1.25 λ.

11 images is from 1.25 λ to 1.25 λ, and the increment between two adjacent images is 0.25 λ. It can be seen that all the PSF images keep nearly the same in spite of different defocus and express the expectative cubic distribution like ideal PSF as shown in Fig. 6(a).

Secondly, the third plate of WT1005-62 resolution patterns is imaged as shown in Fig. 7. There are 25 fringe pattern groups of different space frequency on the plate. The space frequency of the first group is 25 lp/mm while that of the 25th group is 100 lp/mm. The space frequency of one group is $\sqrt[12]{2}$ times of its former group. Because the cut-off frequency of the optical system is 57.2 lp/mm, the 16th group is concerned about which space frequency is about 59.5 lp/mm. Totally 11 images are recorded as shown in Fig. 8, and the positions of image plane are corresponding to the 11 PSF images. Only the images of the 16th group are given for brevity. It can be observed that the image quality stays nearly invariant regardless different image plane position although the image quality is depressed.

According to the wavefront-coding theory, the degraded images obtained by CCD directly are interim and require further restoration. Thus, the final step of the experiment is to restore all the images through the same wiener filter as shown in Fig. 9. The deconvolution core is transferred from the PSF of the nominal image plane (W020 = 0) and applied in the restoration of every image without any change. It can be observed that the definition and the contrast of the restored images are improved. However, the improvement is not as satisfied as expected. It is mainly because the PSF is the image of 20-μm star point not of 8.8-μm one (the theoretical size by computation) and needs to be re-sampled before being applied in the wiener filter. Therefore, some useful information of the PSF, especially in the high-frequency domain may be lost or scrambled, which limits the restoring precision.

In this letter, the alignment and imaging experiment of a space telescope with WFC technology is described. It has been proven that the DOF of the telescope is extended by applying WFC technology and the medial image quality can be well restored. The detailed analysis and comparison of the character of PSF images, original fringe pattern images and its restored images will be described in latter papers. The acquirement of PSF with better accuracy and the proper algorithm towards restored images of higher quality is planned in future work.

This research was supported by the National High Technology Research and Development Program of China (863 Program) (No. 2009AA12Z105). The authors appreciate Dr. Li Fazhi and Dr. Cheng Qiang for their assistance and helpful advice in performing the experiment.

References

1. E. J. Tremblay, J. Rutkowski, I. Tamayo, P. E. X. Silveira, R. A. Stack, R. L. Morrison, M. A. Neifeld, Y. Fainman, and J. E. Ford, Appl. Opt. **46,** 6751 (2007).
2. C. C. Chang and C. C. Lee, Opt. Express **17,** 6245 (2009).
3. G. Muyo, A. Singh, M. Andersson, D. Huckridge, A. Wood, and A. R. Harvey, Opt. Express **17,** 21118 (2009).
4. J. C. James, R. B. Vaughan, J. W. Wood, G. Bennett, R. S. Draper, A. Hastings, J. Stevens, and K. Bryant, in Imaging Systems, OSA technical Digest (CD) (Optical Society of America, 2010) IMB3.
5. J. A. Davis and D. M. Cottrell, Opt. Express **19,** 17677 (2011).
6. M. Somayaji, V. R. Bhakta, and M. P. Christensen, Opt. Express **20,** 1878 (2012).
7. V. R. Bhakta, M. Somayaji, and M. P. Christensen, Appl. Opt. **51**, A17 (2012).
8. Y. Feng and X. Zhang, Opt. Express 17 16809 (2009).
9. M. Larivière-Bastien and S. Thibault, Opt. Lett. **38,** 3830 (2013).
10. G. Saavedra, I. Escobar, R. Martínez-Cuenca, E. Sánchez-Ortiga, and M. Martínez-Corral, Opt. Express **17,** 13810 (2009).
11. A. Harvey, M. Demenikov, G. D. Muyo, and T. Vettenburg, in Frontiers in Optics 2009/Laser Science XXV/Fall 2009 OSA Optics & Photonics Technical Digest, OSA Technical Digest (CD) (Optical Society of America, 2009) FThX2.